Supporting Information

Bonding-antibonding state transition induces multiple electron modulations toward oxygen reduction reaction electrocatalysis

Qi Zhang,[a] Haixia Zhong,[b] Can Chen,[a] Juexian Cao,[c] Liwen Yang[a] and Xiaolin Wei*,[a]

[a] School of Physics and Optoelectronics, Xiangtan University, Hunan, 411105, China.

[b] Faculty of Chemistry and Food Chemistry, Dresden University of Technology, 01062 Dresden, Germany

[c] Hunan Institute of Advanced Sensing and Information Technology, Xiangtan University, Hunan, 411105, China.

*Corresponding authors. E-mail address: xlw@xtu.edu.cn

Table of Contents

Calculated Procedures

As shown in **Fig. S1**, a serials of B-doped Ni-N_4 nanoribbons were constructed. The B atom locates in the edge of nanoribbon. In Ni-N_4-2B-2 and Ni-N_4-B-2, the two-fold coordinated B bonds to one C atom and one N atom. In Ni-N_4-2B-1, the two-fold coordinated B bonds to two C atoms. Besides, the edged C atoms of all nanoribbons were saturated with hydrogen. The formation energies (E_f) of these compounds were calculated to exam their stabilities. The more negative the formation energy means better stability of the compound. And the formation energy was obtained from the following equation:

$$E_f = \frac{E(A_nB_m) - n * E(A) - m * E(B)}{n + m}$$

where $E(A_nB_m)$ is the total energy of the A_nB_m, $E(A)$ and $E(B)$ are the normalized energies of corresponding elements A and B, respectively. As shown in **Fig. S1**, the formation energies of these compounds are negative, indicating a good thermodynamic stability.

The $4e^-$ ORR process under alkaline condition consists of the formation of OOH*, O* and OH* and the OH* desorption, corresponding to the four element reactions as following:

$O_2 + H_2O(l) + e^- \rightarrow OOH^* + OH^-$

$OOH^* + e^- \rightarrow O^* + OH^-$

$O^* + H_2O(l) + e^- \rightarrow OH^* + OH^-$

$OH^* + e^- \rightarrow OH^-$

Where * represents the reaction site. The overall reaction scheme of O_2 reduction to OH^- in alkaline environment is:

$$O_2(g) + 2H_2O(l) + 4e^- \rightarrow 4OH^-$$

Since it is difficult to obtain the exact free energy of OOH, O, and OH radicals in the electrolyte solution, the adsorption free energy ΔGOOH*, ΔGO*, and ΔGOH*, which correspond to OOH*, O*, and OH* adsorptions on surface of catalyst are calculated as follows:

$$\triangle G_{OOH^*} = G_{OOH@cata} + G_{H2O(l)} - G_{cata} - 3G_{OH^-}$$

$$\triangle G_{O^*} = G_{O@cata} + G_{H2O(l)} - G_{cata} - 2G_{OH^-}$$

$$\triangle G_{OH^*} = G_{OH@cata} - G_{cata} - G_{OH^-}$$

The Gibbs free energy of reactions involving electron/proton transfer was calculated based on the computational hydrogen electrode (CHE) model. The Gibbs free energy difference (△G) of each elementary reaction was given by the following equation:

$$\triangle G(U) = \triangle E - \triangle E_{ZPE} + T\triangle S + \triangle G_{Ph} + \triangle G_U$$

where △E is the total energy change obtained from DFT calculations, $\triangle E_{ZPE}$ is the change in zero-point energy, T is temperature (298.15 K) and △S is the change in entropy, $\triangle G_{pH} = k_B T \ln 10 \times pH$, where k_B is the Boltzmann constant, and pH = 14 for 1 M KOH medium, $\triangle G_U = -neU$, where U is the electrode potential with respect to the normal hydrogen electrode, e is the transferred electron, and n is the number of transferred electron.

Hence, the calculated equilibrium potential (U_0) for ORR at pH = 14 was 0.4 V vs NHE where the start state and final state are at the same energy level. The applied limited potential (U_L) is defined as the applied potential where the whole ORR starts to occur.

$U_L = \{-\max[\triangle G_{OOH*}, \triangle G_{O*} - \triangle G_{OOH*}, \triangle G_{OH*} - \triangle G_{O*}, -4.92\ eV - \triangle G_{OH*}]\}/e$

Then the overpotential is equal to the value of U_L minus U_0.

$\eta = U_0 - U_L$

The free energy of $H_2O(l)$ was calculated based on $G_{H2O(g)}$ obtained from DFT calculations and derived as $G_{H2O(l)} = G_{H2O(g)} + RT \times \ln(p/p0)$, where R is the ideal gas constant, T = 298.15K, p = 0.035 bar, and p0 = 1 bar. Due to the limitation of DFT calculations in accurately reflecting the true nature of oxygen molecule with high-spin ground state, the $GO_2(g)$ was derived as $G_{O2(g)} = 2G_{H2O(l)} - 2G_{H2} - 4.92$ eV.

Supplementary Figures

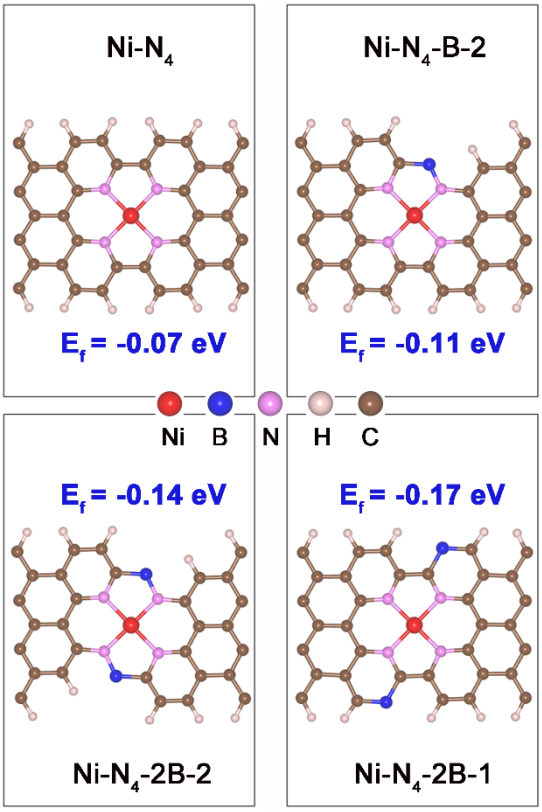

Fig. S1. The calculated models and the corresponding formation energies of Ni-N_4 and B doped Ni-N_4.

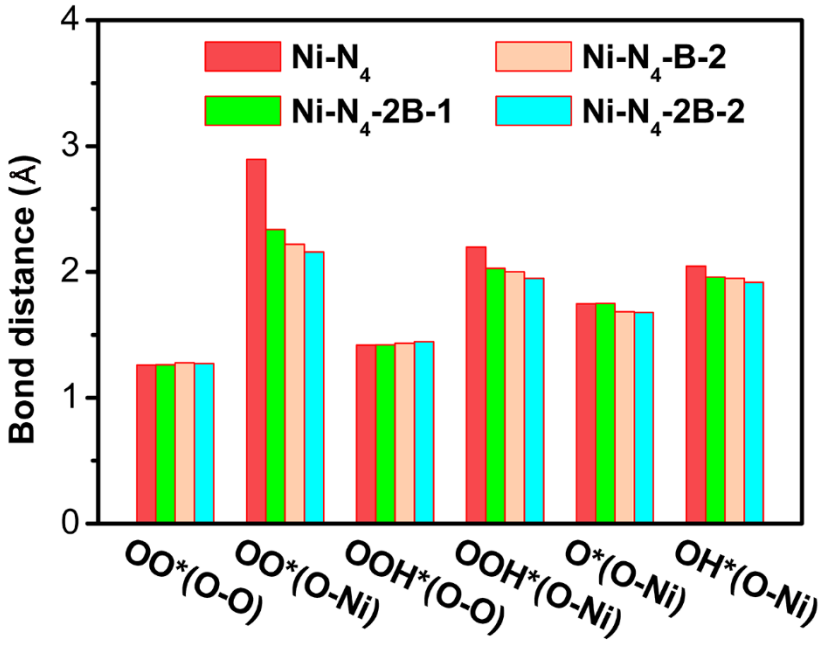

Fig. S2. The bond distances of various O_xH_y for the optimized Ni-N_4 and B doped Ni-N_4.

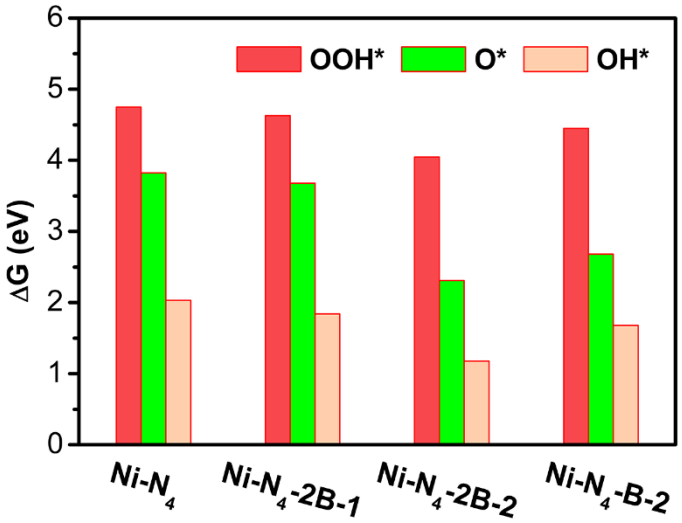

Fig. S3. The adsorption free energy of the intermediates (OOH*, O* and OH*) for Ni-N_4 and B doped Ni-N_4.

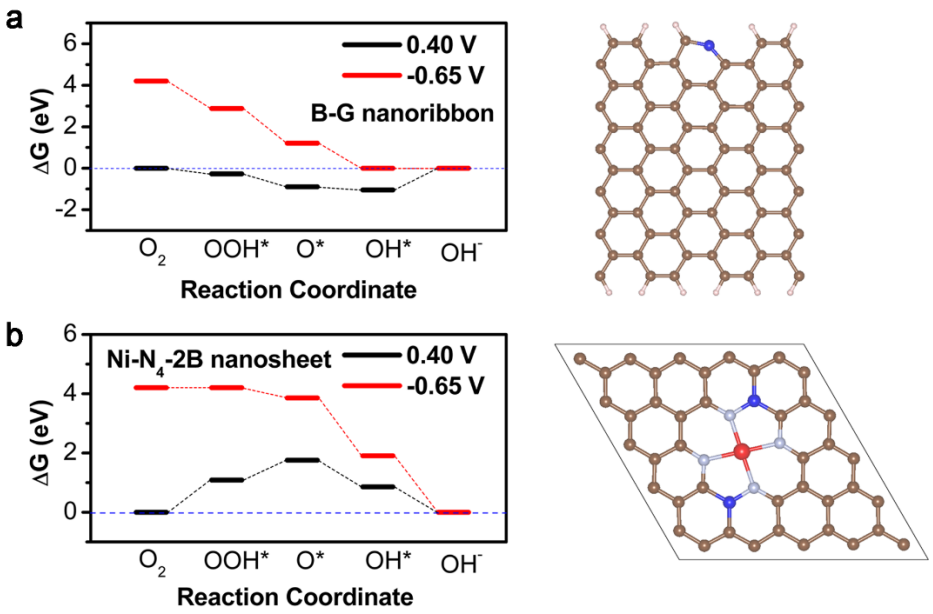

Fig. S4. The free energy diagrams for ORR on the Ni-N_4-2B nanosheet and B-doped graphene nanoribbon.

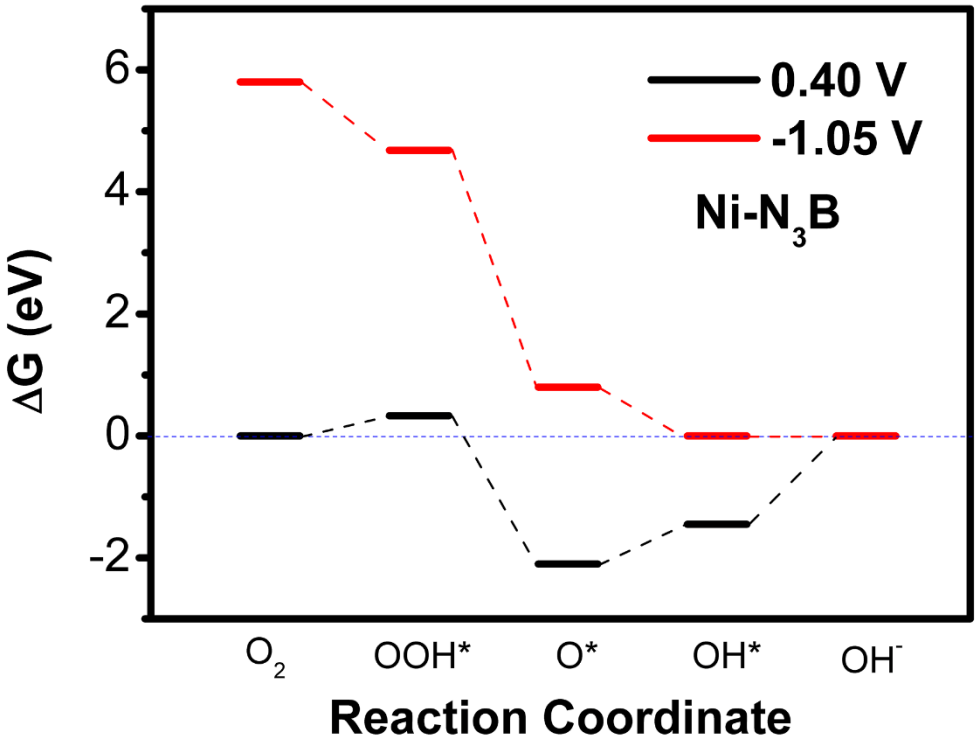

Fig. S5. The free energy diagrams for ORR on the Ni-N_3B.

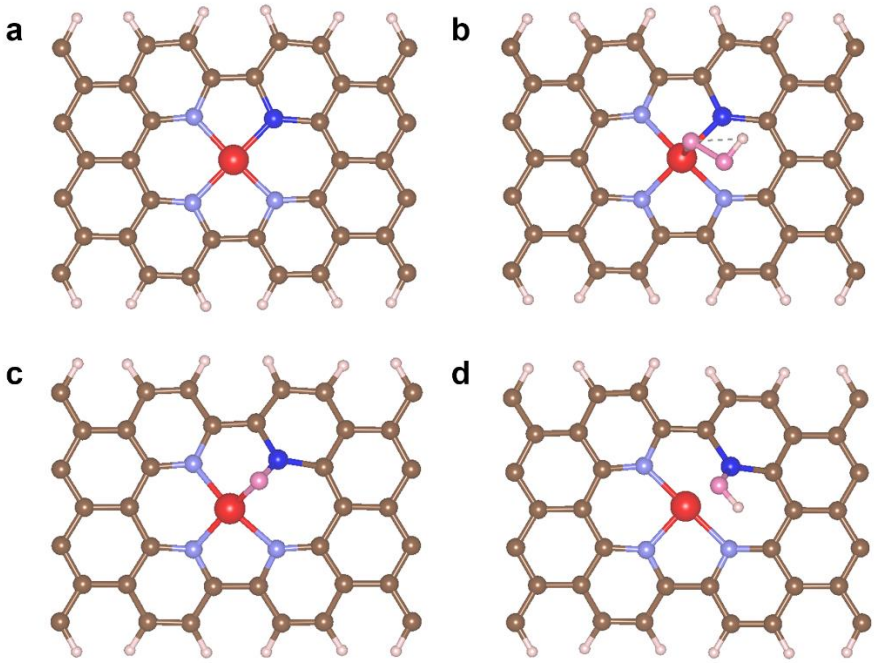

Fig. S6. The calculated models of (a) Ni-N_3B and its intermediates (b-c) toward ORR.

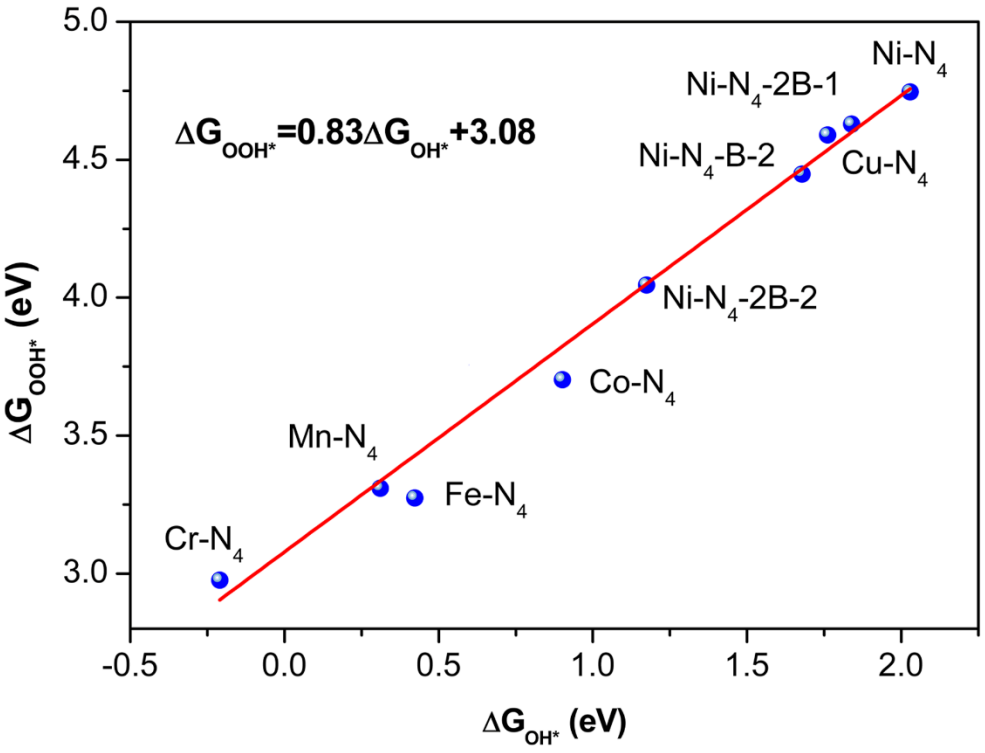

Fig. S7. The scaling relations of ΔG_{OOH*} vs ΔG_{OH*} for various M-N_4 structures and B-doped Ni-N_4 structures.

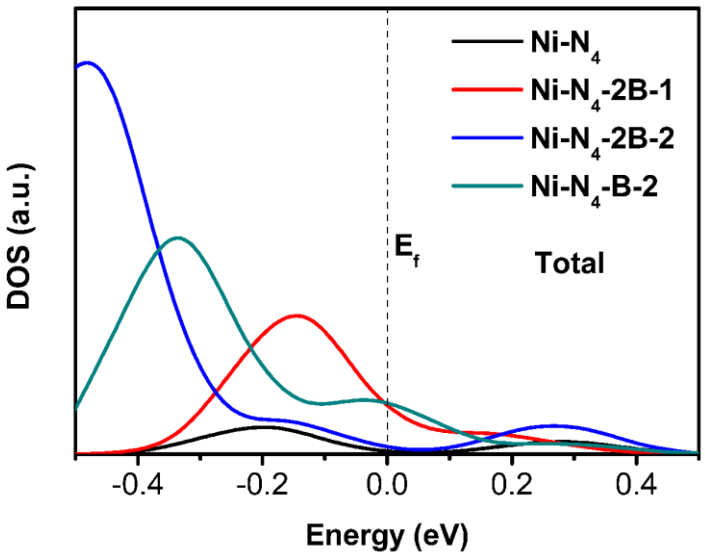

Fig. S8. The total DOS of the B-doped Ni-N_4 systems and Ni-N_4 structure.

Table S1. The ORR catalytic activity of B-doped Ni-N_4 and their similar structures M-N_xC.

Materials	RDS	Overpotential η (V)	References
Ni-N_4	O_2+*+H_2O+e^-→OOH*+OH^-	1.05	This work
Ni-N_4-B-2	O_2+*+H_2O+e^-→OOH*+OH^-	0.75	
Ni-N_4-2B-1	O_2+*+H_2O+e^-→OOH*+OH^-	0.94	
Ni-N_4-2B-2	O_2+*+H_2O+e^-→OOH*+OH^-	0.35	
Ni-N_3B	OH*+e^-→OH^-+*	1.45	
Mn-N_3-Gra	OH*+e^-→OH^-+*	0.56	1
Co-N_3-Gra	OH*+e^-→OH^-+*	0.89	
Ni-N_2	OH*+e^-→OH^-+*	0.43	2
Ni_3(HITP)$_2$	O_2+*+H_2O+e^-→OOH*+OH^-	0.63	3
Co-N_4-G	O_2+*+H_2O+e^-→OOH*+OH^-	0.82	4
Ni-G	O*+H_2O+e^-→OH*+OH^-	1.71	5
Si-G	OH*+e^-→OH^-+*	1.98	
Au-G	O*+H_2O+e^-→OH*+OH^-	0.79	
Fe-G	OH*+e^-→OH^-+*	1.21	
Ag-G	O*+H_2O+e^-→OH*+OH^-	1.08	
Co-G	OH*+e^-→OH^-+*	1.05	
WN_3	O*+H_2O+e^-→OH*+OH^-	1.59	6
WN_4	OH*+e^-→OH^-+*	0.58	
WN_5	OH*+e^-→OH^-+*	0.38	
B-G	O_2+*+H_2O+e^-→OOH*+OH^-	0.72	7
Pt (111)	OH*+e^-→OH^-+*	0.45	8

References

[1] Q. Gao, A DFT study of the ORR on M–N_3 (M = Mn, Fe, Co, Ni, or Cu) co-doped graphene with moiety-patched defects, Ionics, (2019), DOI: 10.1007/s11581-019-03376-9.

[2] S. Kattel, P. Atanassov, B. Kiefer, Density Functional Theory Study of Ni–N_x/C Electrocatalyst for Oxygen Reduction in Alkaline and Acidic Media, J. Phys. Chem. C, 116 (2012) 17378-17383.

[3] F. Sun, X. Chen, Oxygen reduction reaction on $Ni_3(HITP)_2$: A catalytic site that leads to high activity, Electrochem. Commun, 82 (2017) 89-92.

[4] M. Xiao, H. Zhang, Y. Chen, J. Zhu, L. Gao, Z. Jin, J. Ge, Z. Jiang, S. Chen, C. Liu, W. Xing, Identification of binuclear Co_2N_5 active sites for oxygen reduction reaction with more than one magnitude higher activity than single atom CoN_4 site, Nano Energy, 46 (2018) 396-403.

[5] X. Chen, S. Chen, J. Wang, Screening of catalytic oxygen reduction reaction activity of metal-doped graphene by density functional theory, App. Surf. Sci., 379 (2016) 291-295.

[6] Z. Chen, W. Gong, Z. Liu, S. Cong, Z. Zheng, Z. Wang, W. Zhang, J. Ma, H. Yu, G. Li, W. Lu, W. Ren, Z. Zhao, Coordination-controlled single-atom tungsten as a non-3d-metal oxygen reduction reaction electrocatalyst with ultrahigh mass activity, Nano Energy, 60 (2019) 394-403.

[7] Y. Jiao, Y. Zheng, M. Jaroniec, S.Z. Qiao, Origin of the Electrocatalytic Oxygen Reduction Activity of Graphene-Based Catalysts: A Roadmap to Achieve the Best Performance, J. Am. Chem. Soc, 136 (2014) 4394-4403.

[8] J.K. Nørskov, J. Rossmeisl, A. Logadottir, L. Lindqvist, J.R. Kitchin, T. Bligaard, H. Jónsson, Origin of the Overpotential for Oxygen Reduction at a Fuel-Cell Cathode, J. Phys. Chem. B, 108 (2004) 17886-17892.